Research Square

Preprints are preliminary reports that have not undergone peer review.
They should not be considered conclusive, used to inform clinical practice,
or referenced by the media as validated information.

P50 and CNV as Temporal Anchors of Large-Scale Network State Transitions: A Dynamic Connectivity Study in Migraine

Jing Li
The First Hospital of Jilin University
Fei Yin
the Second Hospital of Jilin University
Qingru Chang
The First Hospital of Jilin University
Yongxiang Zhang
Capital Medical University
Qiuxia Deng
The First Hospital of Jilin University
Zhiyuan Sun
Chinese Academy of Science
Qinghua He
Beijing Institute of Technology
Yuan Zhang
Southwest University
Alan Luiz Eckeli
Universidade de S˜ao Paulo
Yudan Lv
lvyd@jlu.edu.cn

The First Hospital of Jilin University

Research Article

Keywords: Migraine, Event-related potential (ERP), P50, CNV, Functional connectivity, Brain network

Posted Date: September 21st, 2026

DOI: https://doi.org/10.21203/rs.3.rs-10852249/v1

License: This work is licensed under a Creative Commons Attribution 4.0 International License.
Read Full License

Additional Declarations: No competing interests reported.

Abstract

Objective

To elucidate the dynamic neural mechanisms underlying migraine-related cognitive impairments from a dual-temporal network perspective by using P50 and CNV as temporal anchors, and to systematically examine abnormal network reorganization during the transition from rest to task in migraine patients.

Methods

High-density EEG source localization was combined with dynamic brain network analysis to capture large-scale network state transitions triggered by P50 and CNV during the transition from rest to task.

Results

We hypothesize that P50 marks an early disengagement between the sensory network and the default mode network, while the evolution of CNV reflects ongoing coordination and resource allocation within the fronto-parietal control network; migraine-related cognitive impairments may stem from delayed, inefficient, or desynchronized state transitions at these critical moments.

Conclusions

This study holds promise for providing mechanobiological biomarkers for network-based precision interventions and for driving a paradigm shift from static regional localization to dynamic system integration.

1. Introduction

Migraine is a complex neurological disorder and one of the leading causes of disability worldwide (Cortel-LeBlanc et al., 2023). Beyond its well-recognized ictal features—such as pulsating headache, photophobia, and nausea—migraine also manifests with cognitive dysfunction, including deficits in attention, processing speed, and executive function (Fernandes et al., 2024; Klepper et al., 2022). The pathophysiological understanding of migraine has evolved considerably beyond the classical trigeminovascular model, increasingly converging on a fundamental neurobiological mechanism: disrupted cortical excitation–inhibition balance and impaired large-scale network interactions (Chever et al., 2021; Mathew & Panonnummal, 2022).

In the cognitive assessment of migraine patients, traditional psychometric instruments (such as the MoCA and MMSE) lack the sensitivity and specificity required to detect subclinical or fluctuating cognitive changes, highlighting the urgent need for objective electrophysiological markers (Farid et al.,

2025). Event-related potentials (ERPs), with their millisecond-level temporal resolution, provide a unique window into the neurodynamic basis of migraine-related cognitive dysfunction (Hassin-Baer et al., 2022; Storozheva et al., 2021). The auditory P50 component is an established indicator of early sensory gating, typically elicited using a paired-click paradigm (S1-S2), reflecting the brain's ability to filter out redundant sensory input (Kim et al., 2020). As demonstrated by Ambrosini et al. (Ambrosini et al., 2001), healthy individuals typically exhibit strong inhibition of the S2 response relative to S1 (S2/S1 ratio < 0.5). In contrast, migraine patients frequently exhibit insufficient inhibition and elevated ratios, indicating impaired early sensory filtering (Li et al., 2026). Furthermore, the Correlated Negative Variation (CNV) is a late slow potential evoked by warning-instruction stimuli, reflecting higher-order cognitive processes such as temporal anticipation, sustained attention, and motor readiness. This study employed the more robust area under the curve (AUC) metric rather than the traditional single-point amplitude, focusing on three function-specific components: the terminal CNV (tCNV), representing the total amount of resources mobilized throughout the preparation process; the late CNV (oCNV), specifically reflecting the sustained coordination capacity of the prefrontal-parietal network; and the post-command negative variant (PINV), reflecting the efficiency of the transition from preparation to execution. As reported by Kropp et al. (P. Kropp & Gerber, 1998), compared to healthy controls, migraine patients exhibit significantly enhanced CNV amplitude, and this elevation persists even during asymptomatic interictal periods (P. Kropp & Gerber, 1995), suggesting dysfunction in cortical excitability regulation and cognitive anticipation.

However, traditional ERP research has largely treated P50 and CNV as isolated time-domain indices, thereby failing to fully elucidate the dynamic, whole-brain network integration that underlies these electrophysiological phenomena(Elverman et al., 2021). Recent advances in network neuroscience have demonstrated that brain function emerges from the flexible, dynamic coordination and switching among large-scale networks(Smallwood et al., 2021). Resting-state functional MRI studies have preliminarily identified aberrant connectivity within core networks in migraine, such as the default mode, salience, and central executive networks(Cankaya et al., 2025; Lei & Zhang, 2021; Xiong et al., 2024). Nevertheless, these resting-state "static snapshots" are fundamentally incapable of revealing how brain networks dynamically reorganize and operate cooperatively on a millisecond timescale under specific cognitive demands—precisely the key to understanding the dynamic nature of migraine cognitive dysfunction.

Therefore, this study aims to link "temporal anchors" with "network states" to uncover the dynamic neural basis of cognitive impairment in migraine. This endeavor not only promises novel mechanistic insights and biomarkers but also embodies a crucial paradigm shift from static correlational analysis toward causal, dynamic systems modeling. We propose an innovative framework that reconceptualizes P50 and CNV as critical temporal anchor points that trigger transitions between large-scale brain network states, thereby enabling the investigation of how these events guide the dynamic reconfiguration from rest to task-engaged states and how this process is disrupted in migraine (Chang et al., 2022; D. Liu et al., 2023; Markett et al., 2022). We hypothesize that P50 not only indexes primary sensory gating but also marks the early initiation of decoupling between sensory networks and the default mode network (Ajunwa et al., 2024), whereas the evolution of CNV reflects the sustained

coordination and resource allocation of the prefrontal-parietal control network. Migraine-related cognitive dysfunction may stem from delayed, inefficient, or desynchronized network-state transitions at these pivotal temporal junctures. By integrating high-density EEG source localization with dynamic brain network analysis, this study strives to bridge the gap from local electrophysiological events to global network dynamics, thereby offering a novel spatiotemporal, "temporal-network" dual-dimension account of cognitive dysfunction in migraine. This framework is expected to provide both mechanistic biomarkers and a theoretical foundation for network-based precision intervention strategies (Bassez et al., 2020; Lu et al., 2024), exemplifying the broader paradigm shift in neuroscience from static regional mapping to dynamic systems integration.

2. Clinical Data and Methods

2.1 Participants

Thirty migraine patients diagnosed in the Department of Neurology, First Hospital of Jilin University, between March 2025 and December 2025 were enrolled as the migraine group (CM group). All patients fulfilled the diagnostic criteria of the International Classification of Headache Disorders, 3rd edition (ICHD-3) and met the eligibility requirements of the present study. Concurrently, 30 age-, sex-, and education-matched healthy volunteers were recruited as the healthy control group (HC group). The study was approved by the Ethics Committee of the First Hospital of Jilin University, and written informed consent was obtained from all participants.

2.1.1 Inclusion Criteria

(1) Absence of any other headache disorders or psychiatric conditions.

(2) Age between 30 and 70 years.

(3) Education level of at least primary school.

(4) Hamilton Anxiety Scale (HAMA) score ≤ 7 and Hamilton Depression Scale (HAMD) score ≤ 8.

(5) No use of psychotropic medications within the preceding 2 weeks.

(6) Right-handedness; no history of smoking, alcohol, or substance abuse.

(7) Recordings were performed during the interictal phase (i.e., > 72 h after cessation of the last migraine attack and > 48 h before onset of the next attack), and all patients were in a medication-free state.

2.1.2 Exclusion Criteria

(1) Headache attributable to an underlying organic disease, severe anxiety, or major depression.

(2) History of neurological injury, including cerebral hemorrhage, traumatic brain injury, brain tumor, or previous brain surgery.

(3) Cognitive impairment confirmed by the Mini-Mental State Examination (MMSE) or the Montreal Cognitive Assessment (MoCA).

(4) Severe hearing impairment.

(5) Receipt of prophylactic anti-migraine treatment.

(6) Inability to cooperate sufficiently to complete the study procedures.

All participants provided written informed consent, and the study protocol was approved by the Ethics Committee of the First Hospital of Jilin University.

2.2 Event-Related Potential and Resting-State EEG Acquisition

2.2.1 ERP Recording

Prior to the P50 and CNV paradigms, all participants completed the MMSE, MoCA, HAMA, and HAMD assessments to exclude cognitive impairment, anxiety, and depression (see Table 1). Recordings were conducted in a dedicated brain function laboratory using a Neuroscan 64-channel EEG system. On the day before the experiment, participants were instructed to ensure adequate rest and to wash their hair. During the experiment, each participant was seated comfortably and fitted with a 64-electrode cap arranged according to the International 10–20 system. The ground electrode was placed at the nasion, and electrodes for recording horizontal and vertical electrooculogram were affixed at appropriate locations. Electrode impedances were kept below 10 kΩ, and the sampling rate was set at 1000 Hz. Prior to recording, the participant was reminded to remain relaxed and focused and to minimize head movements. The P50 task was administered first; upon its completion, a 30-min rest period was provided to ensure that the EEG returned to baseline before the CNV auditory task began. Data were preprocessed using Curry 7 software, re-referenced to the common average reference, and corrected for ocular artifacts, interference, and 50-Hz power line noise. The processed data were stored for subsequent analysis.

2.2.2 P50 Paradigm

P50 data were recorded from 500 ms before S1 to 500 ms after S2, yielding a total epoch of 1500 ms. The temporal resolution was 2.5 ms, resulting in 600 data points per epoch. The P50 component elicited by the first click (S1) was defined as the maximum positive deflection between 30 and 90 ms post-stimulus, with its latency identified in reference to the larger N1 component. The P50 evoked by the second click (S2) was identified within ± 10 ms of the S1 P50 latency. Sensory gating function was

assessed by computing the suppression ratio (S2 amplitude / S1 amplitude), which served as an index of group-level differences in inhibitory capacity.

2.2.3 CNV Paradigm

The CNV paradigm consisted of 40 trials. Each trial comprised a warning stimulus (S1: 50 Hz, 1000 ms) and an imperative stimulus (S2: 50 Hz, up to 3000 ms), separated by an interstimulus interval (ISI) of 3000 ms. Participants were required to press a button immediately upon S2 onset. Recordings spanned from 200 ms before S1 to 4500 ms after S2. The square of the terminal CNV (tCNV-square) was selected as the primary measure to evaluate preparatory, anticipatory, and motor readiness processes in response to the impending S2 and the required behavioral reaction.

2.3 Data Analysis Methods

2.3.1 ERP Data Analysis

Preprocessed data were bandpass filtered between 0.5 and 45 Hz using Curry 7 to attenuate high- and low-frequency noise. For the P50 condition, the analysis epoch of 1500 ms (from 500 ms pre-S1 to 500 ms post-S2) was retained, comprising 600 data points at a temporal resolution of 2.5 ms. For the CNV condition, tCNV-square, oCNV-square, and PINV were analyzed.

2.3.2 Brain Network Connectivity Analysis

Using Curry 7, two-minute epochs of resting-state EEG data immediately before and after the tasks, as well as two-minute epochs of task-state data during the P50 and CNV paradigms, were extracted and converted to EDF format. Coherence analysis was performed with MATLAB R2022a and EEGLAB v2024.0. Coherence coefficients (range: 0–1, with higher values indicating stronger connectivity) were computed for 15 electrode pairs (C3–F3, F4–C4, O1–F3, O2–F4, O1–C3, O2–C4, F4–F3, C3–F4, C4–C3, O1–F4, O1–C4, O2–F3, O2–C3, O2–O1) within four frequency bands: delta (1–4 Hz), theta (4–8 Hz), alpha (8–13 Hz), and beta (13–30 Hz). Group-averaged connectivity matrices and brain network graphs were constructed for the pre-task resting state, the P50 task state, the CNV task state, and the post-task resting state. Between-group differences in coherence coefficients (migraine vs. healthy controls) and within-group differences across task phases were examined. Group-level and intragroup difference network maps were generated to identify functional connectivity topologies exhibiting significant alterations.

2.3.3 Statistical Analysis

Statistical analyses were performed using SPSS version 27.0. For continuous variables, normality was assessed with the Shapiro–Wilk test, and homogeneity of variances was examined with Levene's test. When parametric assumptions were met, between-group comparisons were conducted with independent-samples *t*-tests, and within-group comparisons across multiple phases were performed with repeated-measures analysis of variance (ANOVA; Greenhouse–Geisser correction applied when sphericity was violated). When assumptions were not met, the Mann–Whitney U test and the Friedman

test were employed, respectively. Categorical variables were analyzed using the chi-squared test or Fisher's exact test. A two-tailed *p*-value < 0.05 was considered statistically significant. For post hoc comparisons following repeated-measures ANOVA, Bonferroni correction was applied (adjusted α = 0.0083). Data are presented as mean ± standard deviation (normally distributed) or median (interquartile range) (non-normally distributed).

3. Results

3.1 Evaluation of General Clinical Characteristics

There was no difference in age, education, gender, or the score of HAMA or HAMD between the migraine group and the control group, as listed in Table 1.

Table 1
Evaluation of the general data between CM and HC groups

General clinical data	CM	HC
Sample quantity	30	30
Age(years)	38.28 ± 1.33	38.02 ± 1.36
Male(%)	30.00	33.33
Female(%)	70.00	66.67
HAMA	5.42 ± 1.85	4.81 ± 1.10
HAMD	5.93 ± 1.62	4.25 ± 1.22
Frequency of headache (per month)	6.19 ± 0.788	-
Education	13.02 ± 3.15	13.02 ± 3.26
Drug use during the study	-	-
Note: HAMA, Hamilton Anxiety Rating Scale; HAMD, Hamilton Depression Rating Scale.		

3.2 ERP Data Analysis

3.2.1 Analysis of P50 Latency and Amplitude

Figure1 shows a schematic diagram of P50. The S2/S1 ratio reflects cortical inhibitory capacity; in healthy individuals, this value is below 0.5, whereas in migraine patients, it is above 0.5. Compared with healthy controls, patients exhibited a significantly increased S2/S1 ratio at F3, F4, C3, C4, FZ, FCZ, and CZ (Fig. 2A).Compared with the control group, the patient group exhibited prolonged P50 latencies and a smaller reduction in S2 amplitude. The most prominent positive peak occurring between 30 and 90 milliseconds after stimulation was defined as S1; the patient group showed prolonged S1 latencies at the F3, F4, C3, C4, FZ, FCZ, and CZ electrode sites (Fig. 2B). The P50 component of S2 is defined as the

maximum positive wave occurring within a 10-millisecond window following the S2 latency; in the patient group, S2 latency was prolonged in leads F3, F4, C3, C4, FZ, FCZ, and CZ (Fig. 2C), and see Table 2 for details.

Table 2
Differences of P50 latency and S2/S1 ratio between CM group and HC group (M ± SD).

ERP	Channels	DP	HC	*P*-value
S2/S1	F3	1.10 ± 0.37	0.27 ± 0.19	< 0.001
	F4	1.29 ± 0.19	0.40 ± 0.33	< 0.001
	C3	0.88 ± 0.39	0.44 ± 0.31	< 0.001
	C4	0.80 ± 0.48	0.34 ± 0.28	< 0.001
	FZ	1.10 ± 0.50	0.31 ± 0.21	< 0.001
	FCZ	0.99 ± 0.50	0.41 ± 0.22	< 0.001
	CZ	0.86 ± 0.43	0.40 ± 0.23	< 0.001
S1-latency	F3	75.00 ± 12.80	65.40 ± 14.32	0.08
	F4	75.57 ± 13.61	64.63 ± 14.63	0.04
	C3	77.03 ± 15.06	62.27 ± 10.48	< 0.001
	C4	77.83 ± 15.60	65.13 ± 15.49	0.002
	FZ	75.97 ± 13.92	67.77 ± 13.90	0.026
	FCZ	77.87 ± 15.95	65.13 ± 13.58	0.002
	CZ	77.17 ± 15.72	67.17 ± 15.41	0.016
S2-latency	F3	78.50 ± 12.80	65.40 ± 13.26	< 0.001
	F4	78.70 ± 11.37	63.43 ± 15.49	< 0.001
	C3	76.90 ± 13.79	69.43 ± 16.45	0.062
	C4	78.97 ± 11.36	65.83 ± 14.92	< 0.001
	FZ	78.80 ± 12.22	62.77 ± 13.90	< 0.001
	FCZ	78.43 ± 12.39	61.63 ± 13.58	< 0.001
	CZ	75.93 ± 12.79	67.57 ± 15.23	0.013

Note: Data are presented as mean ± SD. All P-values were derived from a two-tailed independent-samples t-test.

Note

S1 and S2 evoked P50 ERP waveforms in healthy controls and migraine patients. **(A)** shows the healthy control group, while **(B)** depicts the migraine patient group. Using the Cz electrode as an example, this figure displays the P50 component ERP waveforms elicited by paired stimuli (S1, S2) under the paired-click paradigm. The purple waveform represents S1-evoked activity, and the cyan waveform indicates S2-evoked activity. The corresponding dashed lines mark the peak latency and amplitude positions of the P50 component. The superimposed S1 and S2 waveforms visually demonstrate the inhibitory effect of repeated stimulation: In the control group, S2 amplitude is significantly reduced compared to S1, indicating normal sensory gating function. In the migraine group, the inhibitory effect on S2 amplitude is weakened, reflecting impaired sensory gating function.

Note

(A) S2/S1 ratio located in F3, F4, C3, C4, FZ, FCZ, and CZ; **(B)** S1-latency located in F3, F4, C3, C4, FZ, FCZ, and CZ; (C) S2-latency located in F3, F4, C3, C4, FZ, FCZ, and CZ (*$p < 0.05$; **$p < 0.01$; ***$p < 0.001$).

3.2.2 Analysis of CNV Square

Compared with the healthy control group, migraine patients exhibited significantly increased tCNV, oCNV, and PINV areas when performing the CNV task (as shown in Fig. 3). Among these, the PINV is a continuation of the CNV, appearing after S2, reflecting sustained activation following task execution, response uncertainty, or persistent cognitive load. Statistical analysis revealed that the PINV area in the patient group was significantly larger than that in the control group at the CZ, F3, F4, FCZ, O1, O2, and Oz electrodes (Fig. 4A); the tCNV waveform reached a negative peak before S2, representing motor preparation and anticipation, with the patient group exhibiting significantly increased tCNV areas in the CZ, FCZ, and FZ leads (Fig. 4B); the oCNV waveform begins after S1, reflecting attentional orientation toward an impending stimulus, and the patient group similarly exhibited significantly increased oCNV areas in the CZ, FCZ, and FZ leads (Fig. 4C) and see Table 3 for details.

Table 3
Differences of P50 latency and S2/S1 ratio between CM group and HC group (M ± SD).

ERP	Channels	DP	HC	*P*-value
S2/S1	F3	1.10 ± 0.37	0.27 ± 0.19	< 0.001
	F4	1.29 ± 0.19	0.40 ± 0.33	< 0.001
	C3	0.88 ± 0.39	0.44 ± 0.31	< 0.001
	C4	0.80 ± 0.48	0.34 ± 0.28	< 0.001
	FZ	1.10 ± 0.50	0.31 ± 0.21	< 0.001
	FCZ	0.99 ± 0.50	0.41 ± 0.22	< 0.001
	CZ	0.86 ± 0.43	0.40 ± 0.23	< 0.001
S1-latency	F3	75.00 ± 12.80	65.40 ± 14.32	0.08
	F4	75.57 ± 13.61	64.63 ± 14.63	0.04
	C3	77.03 ± 15.06	62.27 ± 10.48	< 0.001
	C4	77.83 ± 15.60	65.13 ± 15.49	0.002
	FZ	75.97 ± 13.92	67.77 ± 13.90	0.026
	FCZ	77.87 ± 15.95	65.13 ± 13.58	0.002
	CZ	77.17 ± 15.72	67.17 ± 15.41	0.016
S2-latency	F3	78.50 ± 12.80	65.40 ± 13.26	< 0.001
	F4	78.70 ± 11.37	63.43 ± 15.49	< 0.001
	C3	76.90 ± 13.79	69.43 ± 16.45	0.062
	C4	78.97 ± 11.36	65.83 ± 14.92	< 0.001
	FZ	78.80 ± 12.22	62.77 ± 13.90	< 0.001
	FCZ	78.43 ± 12.39	61.63 ± 13.58	< 0.001
	CZ	75.93 ± 12.79	67.57 ± 15.23	0.013

Note: Data are presented as mean ± SD. All P-values were derived from a two-tailed independent-samples t-test.

Note

Under repeated auditory stimulation, compare the differences between the migraine group and the control group in terms of CNV latency, CNV amplitude, and area under the CNV curve (CNV square). Specifically, oCNV-Square is defined as the area under the curve from 0 milliseconds to 3000 milliseconds; tCNV-Square is defined as the area under the curve from 200 milliseconds (2800

milliseconds) before S2 to 3000 milliseconds; and PINV is defined as the area under the curve from after S2 (3000 milliseconds) to point C.

Note

(A) PINV-Square located in CZ, F3, F4, FCZ, O1, O2, and OZ; **(B)** tCNV-Square located in CZ, FCZ, and FZ; (C) oCNV-Square located in CZ, FCZ, and FZ (*$p < 0.05$; **$p < 0.01$; ***$p < 0.001$).

3.3 Brain Network Connectivity Analysis

3.3.1 Analysis of Brain Network Connectivity During the Pre-task Resting State Between the Two Groups

Analysis of resting-state EEG functional connectivity in the CM (chronic migraine) group and HC (healthy control) group prior to the task revealed significant differences across multiple frequency bands. In the delta band, functional connectivity between the left frontal lobe and bilateral central regions was significantly enhanced in the CM group compared with the HC group. In the theta band, the CM group showed significantly increased functional connectivity between bilateral frontal lobes, as well as between the left frontal lobe and bilateral central regions, and between the left frontal lobe and bilateral occipital lobes. In the alpha band, the CM group exhibited significantly enhanced connectivity between bilateral frontal lobes, between the left frontal lobe and left central region, and between the left frontal lobe and right occipital lobe. In the beta band, the CM group demonstrated significantly increased functional connectivity between bilateral frontal lobes, between the left frontal lobe and bilateral central regions, and between the left frontal lobe and bilateral occipital lobes (Fig. 6a).

Note

Functional connectivity topology of CM and HC groups across six conditions. (**a**) P50 Pre-task, (**b**) during the P50 task, (**c**) P50 Post-task, (**d**) CNV Pre-task, (**e**) during the CNV task, and (**f**) CNV Post-task. Line thickness indicates the strength of functional connectivity.

Note

Functional connectivity topology of CM and HC groups across six conditions. (**a**) P50 Pre-task, (**b**) during the P50 task, (**c**) P50 Post-task, (**d**) CNV Pre-task, (**e**) during the CNV task, and (**f**) CNV Post-task. Taking panel a as an example, the first row displays the group difference network between the CM and HC groups. Thicker lines denote larger between-group differences; solid lines indicate enhanced functional connectivity in the CM group relative to the HC group, whereas dashed lines indicate reduced functional connectivity in the CM group. The second row presents the topological distribution of functional connections with significant between-group differences.

3.3.2 Analysis of Brain Network Connectivity During the P50 Task Between the CM and HC Groups

Functional connectivity analysis of EEG data recorded during the P50 task in the chronic migraine (CM) group and healthy control (HC) group revealed significant differences in specific frequency bands. In the delta band, the CM group showed enhanced functional connectivity between bilateral frontal lobes, but decreased connectivity between the left frontal lobe and bilateral central regions, as well as between the right frontal lobe and right central region, compared with the HC group. In the theta band, the CM group exhibited significantly reduced functional connectivity between the left frontal lobe and left central region, and between the right frontal lobe and right central region. In the alpha and beta bands, no significant differences were observed between the two groups (Fig. 6b).

3.3.3 Analysis of Brain Network Connectivity During the Post-task Resting State Following the P50 Task Between the CM and HC Groups

Functional connectivity analysis of EEG data recorded during the post-task resting state (after the P50 task) in the chronic migraine (CM) group and healthy control (HC) group revealed significant differences across multiple frequency bands. In the delta band, the CM group showed enhanced functional connectivity between bilateral frontal lobes, but decreased connectivity between the left frontal lobe and bilateral central regions, as well as between the right frontal lobe and right central region, compared with the HC group. In the theta band, the CM group exhibited significantly reduced functional connectivity between the left frontal lobe and bilateral central regions, and between the right frontal lobe and right central region. In the alpha band, the CM group showed increased functional connectivity between bilateral frontal lobes, between the left frontal lobe and bilateral central regions, and between the left frontal lobe and bilateral occipital regions. In the beta band, increased functional connectivity was observed in the CM group between bilateral frontal lobes, between the left frontal lobe and bilateral central regions, and between the left frontal lobe and bilateral occipital regions (Fig. 6c).

3.3.4 Analysis of Brain Network Connectivity During the Pre-task Resting State Before the CNV Task Between the CM and HC Groups

Functional connectivity analysis of resting-state EEG recorded before the CNV task in the chronic migraine (CM) group and healthy control (HC) group revealed the following differences. In the delta band, connectivity between the left frontal lobe and bilateral central regions was significantly enhanced in the CM group compared with the HC group. In the theta band, the CM group showed significantly increased functional connectivity between bilateral frontal lobes, between the left frontal lobe and bilateral central regions, and between the left frontal lobe and bilateral occipital lobes. In the alpha band, the CM group exhibited significantly enhanced connectivity between bilateral frontal lobes, between the left frontal lobe and left central region, and between the left frontal lobe and right occipital lobe. In the beta band, the CM group demonstrated significantly increased connectivity between bilateral frontal lobes, between

the left frontal lobe and bilateral central regions, and between the left frontal lobe and bilateral occipital lobes (Fig. 6d).

3.3.5 Analysis of Brain Network Connectivity During the CNV Task Between the CM and HC Groups

Functional connectivity analysis of EEG recorded during the CNV task in the CM and HC groups revealed the following differences. No significant differences were observed between the two groups in the delta or theta bands. In the alpha band, the CM group showed significantly enhanced functional connectivity between bilateral frontal lobes, between bilateral occipital lobes, between the left frontal lobe and left central region, between the left frontal lobe and bilateral occipital lobes, between the right frontal lobe and left occipital lobe, and between the right central region and right occipital lobe. In the beta band, the CM group exhibited significantly enhanced connectivity between bilateral frontal lobes, between the left frontal lobe and left central region, between the right frontal lobe and left central region, between the left frontal lobe and bilateral occipital lobes, and between the left central region and right occipital lobe (Fig. 6e).

3.3.6 Analysis of Brain Network Connectivity During the Post-task Resting State After the CNV Task Between the CM and HC Groups

Functional connectivity analysis of resting-state EEG recorded after the CNV task in the CM and HC groups revealed the following differences. In the delta band, the CM group showed significantly enhanced connectivity compared with the HC group between bilateral frontal lobes and between the left frontal lobe and bilateral occipital lobes. In the theta band, the CM group exhibited significantly enhanced connectivity between bilateral frontal lobes, between the left frontal lobe and right central region, between the left frontal lobe and bilateral occipital lobes, between the right frontal lobe and right central region, and between the right frontal lobe and bilateral occipital lobes. In the alpha band, the CM group showed significantly enhanced connectivity between bilateral frontal lobes, between bilateral central regions, between the left frontal lobe and bilateral central regions, between the left frontal lobe and right occipital lobe, and between the left central region and right occipital lobe. In the beta band, the CM group demonstrated significantly enhanced connectivity between bilateral frontal lobes, between bilateral central regions, between the left frontal lobe and bilateral central regions, between the left frontal lobe and bilateral occipital lobes, between the right frontal lobe and left central region, and between the left central region and right occipital lobe (Fig. 6f).

3.3.7 Analysis of Brain Network Connectivity Across Different Time Periods in the CM Group

Functional connectivity was analyzed in the CM group across six periods: resting state before the P50 task (Period A), during the P50 task (Period B), resting state after the P50 task (Period C), resting state before the CNV task (Period D), during the CNV task (Period E), and resting state after the CNV task

(Period F). For frequency bands showing statistically significant differences, post-hoc pairwise comparisons were performed. The results are as follows:

(1) Period B vs. Period A:

Functional connectivity in the delta band was significantly decreased between the left frontal lobe and bilateral central regions, between the left frontal lobe and bilateral occipital lobes, and between the right frontal lobe and bilateral central regions; in the theta band, connectivity between the left frontal lobe and bilateral central regions was significantly decreased; in the alpha band, connectivity between the left frontal lobe and bilateral central regions and between the left frontal lobe and bilateral occipital lobes was significantly increased; and in the beta band, connectivity between the left frontal lobe and bilateral central regions was significantly increased (Fig. 7a).

(2) Period B vs. Period C:

The delta band showed significantly decreased connectivity between the left frontal lobe and bilateral central regions and between the left frontal lobe and bilateral occipital lobes in Period B; no significant difference was observed in the theta band; in the alpha band, connectivity between the left frontal lobe and bilateral central regions was significantly decreased in Period B; and in the beta band, connectivity between bilateral frontal lobes, between the left frontal lobe and bilateral central regions, and between the right frontal lobe and right central region was significantly increased in Period B (Fig. 7b).

(3) Period C vs. Period A:

The delta band again showed significantly decreased connectivity between the left frontal lobe and bilateral central regions and between the left frontal lobe and bilateral occipital lobes in Period B; no significant difference was found in the theta band; in the alpha band, connectivity between the right frontal lobe and bilateral central regions was significantly increased in Period B; and no significant difference was observed in the beta band (Fig. 7c).

(4) Period E vs. Period D:

In Period E compared with Period D, the delta band exhibited significantly increased connectivity in Period E between the left frontal lobe and bilateral central regions, between the left frontal lobe and bilateral occipital lobes, between the right frontal lobe and bilateral central regions, between the right frontal lobe and bilateral occipital lobes, and between the left central region and right occipital lobe ($p < 0.05$); in the theta band, connectivity between the left frontal lobe and bilateral occipital lobes was significantly increased in Period E; in the alpha band, connectivity between the left frontal lobe and bilateral occipital lobes, between the left frontal lobe and right central region, and between the right frontal lobe and bilateral occipital lobes was significantly decreased in Period E; and in the beta band, connectivity between the left frontal lobe and bilateral occipital lobes and between the right frontal lobe and bilateral occipital lobes was significantly decreased in Period E (Fig. 7d).

(5) Period E vs. Period F:

The delta band showed significantly increased connectivity in Period E between bilateral frontal lobes, between the left frontal lobe and bilateral central regions, between the left frontal lobe and bilateral occipital lobes, between the right frontal lobe and bilateral central regions, and between the right frontal lobe and bilateral occipital lobes; in the theta band, connectivity was significantly increased in Period E between bilateral frontal lobes, between the left frontal lobe and left central region, between the left frontal lobe and bilateral occipital lobes, between the left central region and left occipital lobe, between the right frontal lobe and right central region, and between the right frontal lobe and right occipital lobe; in the alpha band, connectivity was significantly decreased in Period E between the left frontal lobe and bilateral central regions, between the left frontal lobe and bilateral occipital lobes, between the right frontal lobe and bilateral central regions, and between the right frontal lobe and bilateral occipital lobes; and in the beta band, connectivity was significantly decreased in Period E between the left frontal lobe and bilateral central regions, between the left frontal lobe and left occipital lobe, between the right frontal lobe and left central region, between the right frontal lobe and bilateral occipital lobes, and between the left central region and right occipital lobe (Fig. 7e).

(6) Period F vs. Period D:

In Period F compared with Period D, no significant difference was observed in the delta band; in the theta band, connectivity between the right frontal lobe and bilateral occipital lobes was significantly decreased in Period F with no other significant changes; in the alpha band, connectivity between the left frontal lobe and right central region, between the left frontal lobe and bilateral occipital lobes, between the right frontal lobe and bilateral central regions, and between the right frontal lobe and bilateral occipital lobes was significantly increased in Period F; and no significant differences were found in the beta band (Fig. 7f).

Note

Functional connectivity topologies of the CM group across different periods. (**a**) Period B vs. Period A, (**b**) Period B vs. Period C, (**c**) Period C vs. Period A, (**d**) Period E vs. Period D, (**e**) Period E vs. Period F, and (**f**) Period F vs. Period D. Taking Figure (a) as an example, the first row displays the intergroup difference network between Period B and Period A. Thicker lines indicate greater intergroup differences; solid lines indicate enhanced functional connectivity in Period B relative to Period A, while dashed lines indicate weakened functional connectivity in Period B. The second row presents the distribution of functional connectivity topologies with significant intergroup differences.

3.3.8 Analysis of Brain Network Connectivity Across Different Time Periods in the HC Group

(1) Period B vs. Period A:

In Period B compared with Period A, the delta band showed significantly increased functional connectivity in Period B between bilateral frontal lobes and between the left frontal lobe and bilateral central regions; in the theta band, connectivity was significantly increased between bilateral frontal lobes, between the left frontal lobe and bilateral central regions, and between the left frontal lobe and bilateral occipital lobes; in the alpha band, connectivity was significantly increased between bilateral frontal lobes, between the left frontal lobe and bilateral occipital lobes, and between the left frontal lobe and bilateral central regions; and in the beta band, connectivity was significantly increased between bilateral frontal lobes, between the left frontal lobe and bilateral occipital lobes, and between the left frontal lobe and bilateral central regions (Fig. 8a)

(2) Period B vs. Period C:

In the delta band, functional connectivity between the bilateral frontal lobes and between the left frontal lobe and the bilateral parietal regions was significantly enhanced. In the theta band, functional connectivity between the bilateral frontal lobes, between the left frontal lobe and the bilateral parietal regions, and between the left frontal lobe and the right occipital lobe was significantly enhanced. In the alpha band, functional connectivity was significantly enhanced between the bilateral frontal lobes, the left frontal lobe and the bilateral central regions, and the left frontal lobe and the right occipital lobe. In the beta band, functional connectivity was significantly enhanced between the bilateral frontal lobes, the left frontal lobe and the bilateral central regions, and the left frontal lobe and the right occipital lobe (Fig. 8b).

(3) Period C vs. Period A:

There were no statistically significant differences in the delta, alpha, or beta bands. In the theta band, functional connectivity was significantly enhanced between the left frontal lobe and the right parietal lobe, as well as between the left frontal lobe and the left occipital lobe (Fig. 8c).

(4) Period E vs. Period D:

In the delta band, functional connectivity was significantly enhanced during the E period between the bilateral frontal lobes, the left frontal lobe and bilateral parietal regions, and the left frontal lobe and bilateral occipital lobes. In the theta band, functional connectivity was significantly enhanced during the E period between the bilateral frontal lobes, the left frontal lobe and bilateral parietal regions, and the left frontal lobe and bilateral occipital lobes. In the alpha band, functional connectivity between the right frontal lobe and both occipital lobes was significantly reduced during the E period. In the beta band, functional connectivity between the right frontal lobe and both occipital lobes was significantly reduced during the E period (Fig. 8d).

(5) Period E vs. Period F:

In the delta band, functional connectivity was significantly enhanced during the E period between the bilateral frontal lobes, the left frontal lobe and bilateral parietal regions, and the left frontal lobe and

bilateral occipital lobes. In the theta band, functional connectivity was significantly enhanced during the E period between the left frontal lobe and the right parietal region, and between the left frontal lobe and bilateral occipital lobes. In the alpha band, functional connectivity between the right frontal lobe and both occipital lobes was significantly reduced during the E period. In the beta band, functional connectivity between the right frontal lobe and both occipital lobes was significantly reduced during the E period (Fig. 8e).

(6) Period F vs. Period D:

There were no statistically significant differences in functional connectivity between periods A and D in the delta and beta bands. In the theta band, functional connectivity was significantly enhanced in both frontal lobes and between the left frontal lobe and the left central region. In the alpha band, functional connectivity was significantly enhanced between the left frontal lobe and the left central region (Fig. 8f).

Note

Functional connectivity topologies of the HC group across different periods. (**a**) Period B vs. Period A, (**b**) Period B vs. Period C, (**c**) Period C vs. Period A, (**d**) Period E vs. Period D, (**e**) Period E vs. Period F, and (**f**) Period F vs. Period D. Taking Figure (a) as an example, the first row displays the intergroup difference network between Period B and Period A. Thicker lines indicate greater intergroup differences; solid lines indicate enhanced functional connectivity in Period B relative to Period A, while dashed lines indicate weakened functional connectivity in Period B. The second row presents the distribution of functional connectivity topologies with significant intergroup differences.

4. Discussion

4.1 Analysis of ERP Results

Migraine is a chronic neurological disorder with a very high rate of disability, often accompanied by cognitive impairments, particularly problems with attention and memory. Its pathophysiology involves cortical spreading depression (CSD), a mechanism that disrupts cortical and cerebrovascular function, thereby impairing cognitive function (Kitamura & Imai, 2024). This study utilized the P50 and CNV components of event-related potentials to investigate the neurophysiological mechanisms underlying migraine. The patient and control groups were carefully matched to ensure no significant differences in variables such as age, gender, BMI, and years of education. The results revealed impairments in sensory information processing across multiple brain regions in migraine patients, suggesting widespread deficits in early sensory filtering and gating functions. The results indicate that migraine patients exhibit impairments in sensory information processing across multiple brain regions, suggesting widespread deficits in early sensory filtering and gating functions (Dhaem & Robbins, 2022). P50 appears to depend on the thalamocortical-thalamic circuit regulated by the prefrontal cortex and the inhibitory function of GABAergic interneurons (Coppola, Di Lenola, et al., 2020; Tregellas et al., 2007). In healthy individuals, the second stimulus (S2) is significantly inhibited in paired-stimulus conditions; however, in migraine

patients, reduced GABAergic inhibitory function leads to increased S2 amplitude and a higher S2/S1 ratio. Furthermore, migraine patients exhibit microstructural damage in white matter tracts such as the corpus callosum and the superior longitudinal fasciculus, which impairs information integration between the prefrontal cortex and the sensory cortex, further weakening attentional and inhibitory functions (Coppola, Di Renzo, et al., 2020; Rahimi et al., 2022). Thus, the increased P50 S2/S1 ratio provides electrophysiological evidence of dysfunction in the sensory filtering network during the early stages of migraine (Ambrosini et al., 2003).

With regard to copy number variations (CNVs), this study systematically identified abnormal characteristics in migraine patients. These findings are consistent with those reported by Ning et al. (Ning et al., 2023). We found an increase in CNV area among migraine patients; furthermore, we confirmed that the areas of early oCNV, total tCNV, and late PINV were all significantly larger than those in the healthy control group (with the PINV abnormalities consistent with the findings of Besken et al.), and that these changes exhibited region-specific distribution (Besken et al., 1993). Specifically, increases in oCNV and tCNV were confined to the central and frontal regions (CZ, FCZ, FZ), corresponding to excessive attentional arousal in the early stages of the task and heightened motor readiness in the middle stages, respectively (Bender, Weisbrod, Resch, et al., 2007). The neural basis of this condition can be attributed to cortical hyperexcitability, impaired GABAergic inhibition, and defects in inhibitory control (O'Hare et al., 2023). The increase in PINV was observed across the central frontal region, bilateral frontal regions, and the entire occipital region, suggesting that the patient experiences post-task cognitive disengagement and cross-modal cortical dysfunction (Bender, WeisbrodResch, 2007). These electrophysiological changes are highly consistent with the cognitive fatigue, difficulty shifting attention, and visual sensitivity commonly associated with migraine (Ning et al., 2023). Methodologically, this study addressed the limitations of previous research—which focused solely on amplitude and latency—by incorporating the area dimension of time-integrated signals, thereby validating the critical role of the occipital lobe in the later stages of cognitive processing in migraine (Peter Kropp et al., 2012). These findings provide new evidence for the neurophysiological mechanisms underlying migraine-related cognitive impairments and support the use of CNV area as an effective electrophysiological indicator for assessing patients' cognitive function and cortical excitability (de Lahoz et al., 2023).

4.2 Analysis of Brain Network Connectivity Results

A comprehensive analysis of whole-cycle brain network connectivity during pre-task resting state, task state, and post-task resting state in the P50 task revealed that patients with chronic migraine (CM) exhibited characteristic brain network abnormalities throughout the entire task cycle. Furthermore, this pattern of abnormalities was highly consistent with relevant pathological mechanisms and the findings of previous studies (Y. Liu et al., 2020). In the pre-task resting state, the CM group exhibited generalized functional connectivity enhancements in the delta, theta, alpha, and beta frequency bands between the left frontal lobe and the bilateral central regions. This finding aligns with Woolf's "central sensitization" theory (Woolf, 2011), suggesting that excessive connectivity between the left prefrontal cortex—a key node in descending pain modulation—and the central regions of the somatosensory cortex may lead to

the failure of top-down inhibitory functions (Bushnell et al., 2013). Concurrently, enhanced cross-frequency functional connectivity suggests large-scale integration abnormalities between the sensorimotor network and higher-order cognitive control networks (Filippi & Messina, 2019; Yeh et al., 2023). Furthermore, consistent with Nichols et al.'s findings linking disorganization of theta- and beta-band networks in the fronto-parietal region to working memory deficits (Nichols & Holmes, 2002), this maladaptive neural remodeling may drive the chronic progression of the disease by mediating central sensitization and lowering the arousal threshold (J. Zhang et al., 2016). In the P50 task condition, the CM group exhibited excessive transhemispheric connectivity in the delta band within the prefrontal region, which may reflect compensatory regulation of pain by the bilateral prefrontal cortex, consistent with the findings of Apkarian et al. (Apkarian et al., 2011). Concurrently, the CM group exhibited weakened theta-band functional connectivity between the prefrontal cortex and the central region; given that midline frontal theta oscillations are involved in endogenous selective attention (Knight et al., 1999; Murray et al., 2025), this attenuation suggests a defect in sensory filtering. In the post-task resting state, compared with the healthy control group, the CM group exhibited weakened functional connectivity in the delta and theta bands, while functional connectivity in the alpha and beta bands was enhanced. This reflects abnormally rapid desynchronization of the thalamocortical pain network, as well as excessive cortical inhibition and higher-order regulatory compensation initiated to compensate for sensory gating deficits, suggesting that CM patients exhibit post-task cortical dysregulation (Tu et al., 2019). The aforementioned brain network abnormalities spanning the entire task cycle constitute the core feature of cortical excitation-inhibition imbalance in CM patients, providing multi-temporal and multi-frequency electrophysiological evidence for the mechanisms underlying their pathogenesis and chronicity.

In the CNV task, the CM group exhibited widespread enhancement of functional connectivity in the alpha and beta bands. Previous studies have shown that alpha-band activity is negatively correlated with default mode network (DMN) activity; therefore, CM patients may need to enhance alpha-band connectivity during task performance to suppress DMN activity, thereby maintaining task focus and preventing endogenous interference (Jensen & Mazaheri, 2010). Beta-band oscillations, on the other hand, are closely associated with sustained attention, working memory maintenance, and descending pain modulation; thus, CM patients must rely on stronger beta-band connectivity to counteract the depletion of attentional resources and pain interference caused by central sensitization, while simultaneously compensating for deficiencies in descending pain modulation (Park & Reuter-Lorenz, 2009). During post-task resting-state conditions, the CM group exhibited widespread enhancements in functional connectivity across the delta-to-beta frequency bands between the prefrontal cortex and the sensorimotor and visual cortices, reflecting task-induced widespread neuroplastic changes (Engel & Fries, 2010). This enhancement involves multiple brain regions and networks, suggesting that neural compensation in the CM group exhibits broad-scale coordination rather than being limited to the reorganization of local brain regions; while this network-wide coordinated enhancement may help maintain brain homeostasis, it may also imply reduced neural regulatory flexibility and imbalanced compensatory efficiency in patients, which in turn is associated with abnormalities in cognitive and emotional regulation (Parsons et al., 2022).

4.3 Analysis of Results Across Different Phases of Brain Network Connectivity

Based on the changes in functional connectivity across different phases and frequency bands of the task in the CM group, the core pathological feature consistently revolves around “brain network rigidity,” which can be summarized in chronological order as follows. In the P50 task, the three phases—A (pre-task resting state), B (task state), and C (post-task resting state)—form a complete closed loop of abnormal responses, primarily reflecting "deficits in sensory gating and insufficient compensatory capacity," which is consistent with the conclusions of Harmony T et al. (F. J. Hsiao et al., 2018). This study found that excessive hyperactivity in the delta/theta slow-wave bands and insufficient inhibition in the alpha/beta fast-wave bands during Phase A constitute the core baseline pathological basis for the sustained activation of the pain network and cross-modal sensory hypersensitivity in CM patients. Previous studies have shown that the functional topology of brain networks undergoes dynamic reorganization during the transition from rest to task states. During Period B in this study, the CM group exhibited only a passive regulatory pattern characterized by passive inhibition of slow waves and localized compensation of fast waves; moreover, the magnitude and scope of this regulation were significantly weaker than those in the HC group, further highlighting sensory gating deficits (W. Zhang et al., 2020). Period C, on the other hand, presented passive rebound of slow waves, sustained inhibition in the theta band, sustained compensatory enhancement in the alpha band, and only localized recovery in the beta band, directly reflecting brain network rigidity and insufficient regulatory flexibility (Zou et al., 2021).

Building on this, the three periods—D (pre-task resting state), E (task state), and F (post-task resting state)—in the CNV task constitute another complete closed loop of abnormal responses, primarily reflecting "insufficient regulatory precision and marked passive compensation." These findings complement the abnormal responses observed in the P50 task, collectively revealing the universality and task-specificity of brain network abnormalities in CM patients. Specifically, Period D continued the baseline characteristics of Period A—"excessive slow-wave activity and insufficient fast-wave inhibition/regulation"—laying the foundation for attention regulation deficits (F.-J. Hsiao et al., 2022); Phase E, driven by task demands such as active attention, anticipation, and motor preparation, exhibits a passive compensatory pattern characterized by widespread enhancement of slow waves and widespread attenuation of fast waves. Brain regions showing no significant intergroup differences are primarily concentrated in non-core pathways, indicating a dual regulatory deficit in the core pathways of CM patients (Maier et al., 2011). During Phase F, differential rebound was observed across frequency bands, and brain regions showing no significant differences highly overlapped with those in Phase E. The core pathway failed to rapidly return to normal baseline levels, further confirming the persistence of brain network rigidity (Zou et al., 2021).

In stark contrast, the core characteristics of the brain network in the healthy control (HC) group lie in the precision and dynamic flexibility of regulation. As demonstrated by studies by Ekman et al. (Ekman et al.,

2012) and Cole et al. (Cole et al., 2014), the healthy brain does not rely on generalized activation or passive inhibition; instead, it efficiently completes tasks through targeted regulation of core pathways and rapidly returns to baseline levels upon task completion. Specifically, during the P50 task, the HC group exhibited a pattern of "resting-state stability → precise activation of core pathways during the task (enhanced slow waves, bidirectional modulation of fast waves) → rapid post-task reset" during periods A–C (Shen et al., 2020), perfectly demonstrating the normal function of sensory gating; during the CNV task, the pattern of "resting-state stability → precise modulation of core pathways during the task (enhanced slow waves, desynchronization of fast waves) → rapid post-task reset," precisely matching the task demands of active attention, stimulus anticipation, and motor preparation (Teodoro et al., 2020). This physiological regulation pattern stood in stark contrast to the abnormal responses observed in the CM group. Intergroup comparisons further corroborated the view proposed by Harmony T et al. [40] regarding the specificity of brain network abnormalities in CM patients, and provided a reliable reference for pathological mechanisms such as impaired brain network reorganization, defective sensory gating, and abnormal attentional regulation (Harmony, 2013).

5. Conclusions

In summary, this study revealed dynamic abnormalities in brain network connectivity in CM patients through a multi-task paradigm, offering a new perspective for understanding their pathological mechanisms. Changes in brain network connectivity patterns before and after the task may serve as biomarkers for evaluating the efficacy of cognitive interventions, providing a basis for developing personalized treatment plans.

However, this study also has certain limitations. First, the small sample size and the absence of subgroup stratification may have masked the specific neural mechanisms underlying different migraine subtypes. Second, functional connectivity analysis based on coherence coefficients cannot provide information on the direction of information flow; future studies should incorporate methods such as effective connectivity or causal models to further deepen our understanding. Finally, the current findings have not yet been translated into clinical diagnostic tools; it is necessary to develop predictive models integrating electrophysiological and clinical features to facilitate practical application. Future research will further deepen our understanding of the underlying mechanisms and promote the translation of these findings through increased sample size, multimodal integration, and clinical validation.

Declarations

Competing interests

The author(s) declared no conflicts of interest with respect to the research, authorship, funding, and/or publication of this article.

Authors' Contributions

J.L. and Y.D.L. conceived and designed the research. J.L. performed data acquisition, data analysis and interpretation of experimental results. F.Y., Q.R.C., Q.X.D. participated in subject recruitment and clinical data collection. Z.Y.S. provided technical support for EEG signal processing. Q.H.H., Y.Z. offered theoretical guidance for brain-network analysis. A.L.E. revised the manuscript and polished academic expression. Y.X.Z. gave critical comments on clinical interpretation of migraine findings. J.L. drafted the original manuscript. Y.D.L. critically revised the manuscript. All authors read and approved the final version of the manuscript.

Funding

The Funding was supported in part by the National Key Research and Development Program of China (2022ZD0210500), the Jilin Medical and Health Special Project (JLSRCZX2026-01), and Jilin University Collaborative Project (3R2260126428).

Acknowledgments

Thank you, Ms. Lv, for your affirmation and guidance on this topic. I would also like to thank the scholars in the references, whose research results provide an important foundation for this paper.

Method compliance statement

All data generated or analysed during this study are included in this published article and its supplementary information files.

References

1. Ajunwa, C. C., Zhang, J., Collin, G., Keshavan, M. S., Tang, Y., Zhang, T., . . . Whitfield-Gabrieli, S. (2024). Dissociable Default Mode Network Connectivity Patterns Underlie Distinct Symptoms in Psychosis Risk. bioRxiv. doi:10.1101/2024.10.25.620271
2. Ambrosini, A., de Noordhout, A. M., Sándor, P. S., & Schoenen, J. (2003). Electrophysiological studies in migraine: a comprehensive review of their interest and limitations. Cephalalgia, 23 Suppl 1, 13-31. doi:10.1046/j.1468-2982.2003.00571.x
3. Ambrosini, A., De Pasqua, V., Afra, J., Sandor, P. S., & Schoenen, J. (2001). Reduced gating of middle-latency auditory evoked potentials (P50) in migraine patients: another indication of abnormal sensory processing? Neurosci Lett, 306(1-2), 132-134. doi:10.1016/s0304-3940(01)01871-7
4. Apkarian, V. A., Hashmi, J. A., & Baliki, M. N. (2011). Pain and the brain: specificity and plasticity of the brain in clinical chronic pain. Pain, 152(3 Suppl), S49-s64. doi:10.1016/j.pain.2010.11.010
5. Bassez, I., Van de Steen, F., Ricci, K., Vecchio, E., Gentile, E., Marinazzo, D., & de Tommaso, M. (2020). Dynamic Causal Modelling of the Reduced Habituation to Painful Stimuli in Migraine: An EEG Study. Brain Sci, 10(10). doi:10.3390/brainsci10100712

6. Bender, S., Weisbrod, M., & Resch, F. (2007). Stereotyped topography of different elevated contingent negative variation components in children with migraine without aura points towards a subcortical dysfunction. Pain, 127, 221-233. doi:10.1016/j.pain.2006.08.017
7. Bender, S., Weisbrod, M., Resch, F., & Oelkers-Ax, R. (2007). Stereotyped topography of different elevated contingent negative variation components in children with migraine without aura points towards a subcortical dysfunction. 127(3), 221-233. doi:10.1016/j.pain.2006.08.017
8. Besken, E., Pothmann, R., & Sartory, G. (1993). Contingent negative variation in childhood migraine. Cephalalgia, 13(1), 42-43. doi:10.1046/j.1468-2982.1993.1301042.x
9. Bushnell, M. C., Ceko, M., & Low, L. A. (2013). Cognitive and emotional control of pain and its disruption in chronic pain. Nat Rev Neurosci, 14(7), 502-511. doi:10.1038/nrn3516
10. Cankaya, S., Ayyildiz, B., Sayman, D., Duran, U., Ucak, D., Karaca, R., . . . Yulug, B. (2025). Hippocampal connectivity dynamics and volumetric alterations predict cognitive status in migraine: A resting-state fMRI study. Neuroimage, 305, 120961. doi:10.1016/j.neuroimage.2024.120961
11. Chang, Q., Li, C., Zhang, J., & Wang, C. (2022). Dynamic brain functional network based on EEG microstate during sensory gating in schizophrenia. J Neural Eng, 19(2). doi:10.1088/1741-2552/ac5266
12. Chever, O., Zerimech, S., Scalmani, P., Lemaire, L., Pizzamiglio, L., Loucif, A., . . . Mantegazza, M. (2021). Initiation of migraine-related cortical spreading depolarization by hyperactivity of GABAergic neurons and NaV1.1 channels. J Clin Invest, 131(21). doi:10.1172/jci142203
13. Cole, M. W., Bassett, D. S., Power, J. D., Braver, T. S., & Petersen, S. E. (2014). Intrinsic and task-evoked network architectures of the human brain. Neuron, 83(1), 238-251. doi:10.1016/j.neuron.2014.05.014
14. Coppola, G., Di Lenola, D., Abagnale, C., Ferrandes, F., Sebastianelli, G., Casillo, F., . . . Pierelli, F. (2020). Short-latency afferent inhibition and somato-sensory evoked potentials during the migraine cycle: surrogate markers of a cycling cholinergic thalamo-cortical drive? J Headache Pain, 21(1), 34. doi:10.1186/s10194-020-01104-7
15. Coppola, G., Di Renzo, A., Tinelli, E., Petolicchio, B., Di Lorenzo, C., Parisi, V., . . . Pierelli, F. (2020). Patients with chronic migraine without history of medication overuse are characterized by a peculiar white matter fiber bundle profile. J Headache Pain, 21(1), 92. doi:10.1186/s10194-020-01159-6
16. Cortel-LeBlanc, M. A., Orr, S. L., Dunn, M., James, D., & Cortel-LeBlanc, A. (2023). Managing and Preventing Migraine in the Emergency Department: A Review. Ann Emerg Med, 82(6), 732-751. doi:10.1016/j.annemergmed.2023.05.024
17. de Lahoz, M. E., Barjola, P., Peláez, I., Ferrera, D., Fernandes-Magalhaes, R., & Mercado, F. (2023). Unveiling the Role of Contingent Negative Variation (CNV) in Migraine: A Review of Electrophysiological Studies in Adults and Children. Biomedicines, 11(11). doi:10.3390/biomedicines11113030
18. Dhaem, O., & Robbins, M. (2022). Cognitive Impairment in Primary and Secondary Headache Disorders. Current Pain and Headache Reports, 26, 391-404. doi:10.1007/s11916-022-01039-5

19. Ekman, M., Derrfuss, J., Tittgemeyer, M., & Fiebach, C. J. (2012). Predicting errors from reconfiguration patterns in human brain networks. Proc Natl Acad Sci U S A, 109(41), 16714-16719. doi:10.1073/pnas.1207523109
20. Elverman, K. H., Paitel, E. R., Figueroa, C. M., McKindles, R. J., & Nielson, K. A. (2021). Event-Related Potentials, Inhibition, and Risk for Alzheimer's Disease Among Cognitively Intact Elders. J Alzheimers Dis, 80(4), 1413-1428. doi:10.3233/jad-201559
21. Engel, A. K., & Fries, P. (2010). Beta-band oscillations--signalling the status quo? Curr Opin Neurobiol, 20(2), 156-165. doi:10.1016/j.conb.2010.02.015
22. Farid, M. A., Zeinhom, M. G., Ahmed, S. R., & Ramadan, E. S. (2025). Factors influencing the occurrence and characteristics of white matter hyperintensities on the brain imaging of migraine patients. Neurol Sci, 46(10), 5253-5262. doi:10.1007/s10072-025-08373-7
23. Fernandes, C., Dapkute, A., Watson, E., Kazaishvili, I., Chądzyński, P., Varanda, S., . . . Lampl, C. (2024). Migraine and cognitive dysfunction: a narrative review. J Headache Pain, 25(1), 221. doi:10.1186/s10194-024-01923-y
24. Filippi, M., & Messina, R. (2019). The Chronic Migraine Brain: What Have We Learned From Neuroimaging? Front Neurol, 10, 1356. doi:10.3389/fneur.2019.01356
25. Harmony, T. (2013). The functional significance of delta oscillations in cognitive processing. Front Integr Neurosci, 7, 83. doi:10.3389/fnint.2013.00083
26. Hassin-Baer, S., Cohen, O. S., Israeli-Korn, S., Yahalom, G., Benizri, S., Sand, D., . . . Peremen, Z. (2022). Identification of an early-stage Parkinson's disease neuromarker using event-related potentials, brain network analytics and machine-learning. PLoS One, 17(1), e0261947. doi:10.1371/journal.pone.0261947
27. Hsiao, F.-J., Chen, W.-T., Pan, L.-L. H., Liu, H.-Y., Wang, Y.-F., Chen, S.-P., . . . Wang, S.-J. (2022). Resting-state magnetoencephalographic oscillatory connectivity to identify patients with chronic migraine using machine learning. The Journal of Headache and Pain, 23(1), 130. doi:10.1186/s10194-022-01500-1
28. Hsiao, F. J., Wang, S. J., Lin, Y. Y., Fuh, J. L., Ko, Y. C., Wang, P. N., & Chen, W. T. (2018). Somatosensory gating is altered and associated with migraine chronification: A magnetoencephalographic study. Cephalalgia, 38(4), 744-753. doi:10.1177/0333102417712718
29. Jensen, O., & Mazaheri, A. (2010). Shaping functional architecture by oscillatory alpha activity: gating by inhibition. Front Hum Neurosci, 4, 186. doi:10.3389/fnhum.2010.00186
30. Kim, H. K., Blumberger, D. M., & Daskalakis, Z. J. (2020). Neurophysiological Biomarkers in Schizophrenia—P50, Mismatch Negativity, and TMS-EMG and TMS-EEG. Volume 11 - 2020. doi:10.3389/fpsyt.2020.00795
31. Kitamura, E., & Imai, N. (2024). Molecular and Cellular Neurobiology of Spreading Depolarization/Depression and Migraine: A Narrative Review. Int J Mol Sci, 25(20), 11163. http://europepmc.org/abstract/MED/39456943
32. https://doi.org/10.3390/ijms252011163

33. https://europepmc.org/articles/PMC11508361
34. https://europepmc.org/articles/PMC11508361?pdf=render doi:10.3390/ijms252011163
35. Klepper, J. E., Sebrow, L., Rosen, N. L., & Seng, E. K. (2022). Cogniphobia and neuropsychological functioning in migraine. Neuropsychology, 36(5), 433-442. doi:10.1037/neu0000808
36. Knight, R. T., Staines, W. R., Swick, D., & Chao, L. L. (1999). Prefrontal cortex regulates inhibition and excitation in distributed neural networks. Acta Psychol (Amst), 101(2-3), 159-178. doi:10.1016/s0001-6918(99)00004-9
37. Kropp, P., & Gerber, W. D. (1995). Contingent negative variation during migraine attack and interval: evidence for normalization of slow cortical potentials during the attack. Cephalalgia, 15(2), 123-128; discussion 178-129. doi:10.1046/j.1468-2982.1995.015002123.x
38. Kropp, P., & Gerber, W. D. (1998). Prediction of migraine attacks using a slow cortical potential, the contingent negative variation. Neurosci Lett, 257(2), 73-76. doi:10.1016/s0304-3940(98)00811-8
39. Kropp, P., Brecht, I., Niederberger, U., Kowalski, J., Schröder, D., Thome, J., . . . Gerber, W.-D. (2012). Time-dependent post-imperative negative variation indicates adaptation and problem solving in migraine patients. J Neural Transm (Vienna), 119, 1213-1221. doi:10.1007/s00702-012-0843-6
40. Lei, M., & Zhang, J. (2021). Brain function state in different phases and its relationship with clinical symptoms of migraine: an fMRI study based on regional homogeneity (ReHo). Ann Transl Med, 9(11), 928. doi:10.21037/atm-21-2097
41. Li, J., Zhang, Y., Li, H., Liu, C., Sun, Z., Fu, Y., . . . Lv, Y. (2026). A study on cortical habituation based on event-related potential P50 and CNV. Volume 17 - 2026. doi:10.3389/fneur.2026.1787063
42. Liu, D., Cao, T., Wang, Q., Zhang, M., Jiang, X., & Sun, J. (2023). Construction and analysis of functional brain network based on emotional electroencephalogram. Med Biol Eng Comput, 61(2), 357-385. doi:10.1007/s11517-022-02708-8
43. Liu, Y., Chen, Y., Liang, X., Li, D., Zheng, Y., Zhang, H., . . . Qiu, S. (2020). Altered Resting-State Functional Connectivity of Multiple Networks and Disrupted Correlation With Executive Function in Major Depressive Disorder. Front Neurol, 11, 272. doi:10.3389/fneur.2020.00272
44. Lu, Q., Jia, Z., & Gu, H. (2024). Association between brain resting-state functional activities and migraine: a bidirectional mendelian randomization study. Sci Rep, 14(1), 23901. doi:10.1038/s41598-024-74745-2
45. Maier, J., Sebastian, I., Weisbrod, M., Freitag, C. M., Resch, F., & Bender, S. (2011). Cortical inhibition at rest and under a focused attention challenge in adults with migraine with and without aura. Cephalalgia, 31(8), 914-924. doi:10.1177/0333102411408627
46. Markett, S., Nothdurfter, D., Focsa, A., Reuter, M., & Jawinski, P. (2022). Attention networks and the intrinsic network structure of the human brain. Hum Brain Mapp, 43(4), 1431-1448. doi:10.1002/hbm.25734
47. Mathew, A. A., & Panonnummal, R. (2022). Cortical spreading depression: culprits and mechanisms. Exp Brain Res, 240(3), 733-749. doi:10.1007/s00221-022-06307-9

48. Murray, A., Zerroug, Y., Soulières, I., & Saint-Amour, D. (2025). The Role of Fronto-Central Theta Oscillations in Inter-Sensory Selective Attention. Psychophysiology, 62(4), e70055. doi:10.1111/psyp.70055
49. Nichols, T. E., & Holmes, A. P. (2002). Nonparametric permutation tests for functional neuroimaging: a primer with examples. Hum Brain Mapp, 15(1), 1-25. doi:10.1002/hbm.1058
50. Ning, J., Zhang, Y., Wang, Y., Liu, C., Cheng, Y., Zhu, M., . . . Lv, Y. (2023). Exploring the cortical habituation in migraine patients based on contingent negative variation. Volume 14 - 2023. doi:10.3389/fneur.2023.1226554
51. O'Hare, L., Tarasi, L., Asher, J. M., Hibbard, P. B., & Romei, V. (2023). Excitation-Inhibition Imbalance in Migraine: From Neurotransmitters to Brain Oscillations. Int J Mol Sci, 24(12). doi:10.3390/ijms241210093
52. Park, D. C., & Reuter-Lorenz, P. (2009). The adaptive brain: aging and neurocognitive scaffolding. Annu Rev Psychol, 60, 173-196. doi:10.1146/annurev.psych.59.103006.093656
53. Parsons, N., Ugon, J., Morgan, K., Shelyag, S., Hocking, A., Chan, S. Y., . . . Caeyenberghs, K. (2022). Structural-functional connectivity bandwidth of the human brain. Neuroimage, 263, 119659. doi:10.1016/j.neuroimage.2022.119659
54. Rahimi, R., Dolatshahi, M., Abbasi-Feijani, F., Momtazmanesh, S., Cattarinussi, G., Aarabi, M. H., & Pini, L. (2022). Microstructural white matter alterations associated with migraine headaches: a systematic review of diffusion tensor imaging studies. Brain Imaging Behav, 16(5), 2375-2401. doi:10.1007/s11682-022-00690-1
55. Shen, C. L., Chou, T. L., Lai, W. S., Hsieh, M. H., Liu, C. C., Liu, C. M., & Hwu, H. G. (2020). P50, N100, and P200 Auditory Sensory Gating Deficits in Schizophrenia Patients. Front Psychiatry, 11, 868. doi:10.3389/fpsyt.2020.00868
56. Smallwood, J., Bernhardt, B. C., Leech, R., Bzdok, D., Jefferies, E., & Margulies, D. S. (2021). The default mode network in cognition: a topographical perspective. Nat Rev Neurosci, 22(8), 503-513. doi:10.1038/s41583-021-00474-4
57. Storozheva, Z. I., Akhapkin, R. V., Bolotina, O. V., Korendrukhina, A., Novototsky-Vlasov, V. Y., Shcherbakova, I. V., & Kirenskaya, A. V. (2021). Sensorimotor and sensory gating in depression, anxiety, and their comorbidity. World J Biol Psychiatry, 22(3), 183-193. doi:10.1080/15622975.2020.1770859
58. Teodoro, T., Koreki, A., Meppelink, A. M., Little, S., Nielsen, G., Macerollo, A., . . . Edwards, M. J. (2020). Contingent negative variation: a biomarker of abnormal attention in functional movement disorders. Eur J Neurol, 27(6), 985-994. doi:10.1111/ene.14189
59. Tregellas, J. R., Davalos, D. B., Rojas, D. C., Waldo, M. C., Gibson, L., Wylie, K., . . . Freedman, R. (2007). Increased hemodynamic response in the hippocampus, thalamus and prefrontal cortex during abnormal sensory gating in schizophrenia. Schizophr Res, 92(1-3), 262-272. doi:10.1016/j.schres.2006.12.033

60. Tu, Y., Fu, Z., Zeng, F., Maleki, N., Lan, L., Li, Z., . . . Kong, J. (2019). Abnormal thalamocortical network dynamics in migraine. Neurology, 92(23), e2706-e2716. doi:10.1212/wnl.0000000000007607
61. Woolf, C. J. (2011). Central sensitization: implications for the diagnosis and treatment of pain. Pain, 152(3 Suppl), S2-s15. doi:10.1016/j.pain.2010.09.030
62. Xiong, X., Dai, L., Chen, W., Lu, J., Hu, C., Zhao, H., & Ke, J. (2024). Dynamics and concordance alterations of regional brain function indices in vestibular migraine: a resting-state fMRI study. J Headache Pain, 25(1), 1. doi:10.1186/s10194-023-01705-y
63. Yeh, C. H., Zhang, C., Shi, W., Lo, M. T., Tinkhauser, G., & Oswal, A. (2023). Cross-Frequency Coupling and Intelligent Neuromodulation. Cyborg Bionic Syst, 4, 0034. doi:10.34133/cbsystems.0034
64. Zhang, J., Su, J., Wang, M., Zhao, Y., Yao, Q., Zhang, Q., . . . Du, X. (2016). Increased default mode network connectivity and increased regional homogeneity in migraineurs without aura. J Headache Pain, 17(1), 98. doi:10.1186/s10194-016-0692-z
65. Zhang, W., Tang, F., Zhou, X., & Li, H. (2020). Dynamic Reconfiguration of Functional Topology in Human Brain Networks: From Resting to Task States. Neural Plast, 2020, 8837615. doi:10.1155/2020/8837615
66. Zou, Y., Tang, W., Qiao, X., & Li, J. (2021). Aberrant modulations of static functional connectivity and dynamic functional network connectivity in chronic migraine. Quant Imaging Med Surg, 11(6), 2253-2264. doi:10.21037/qims-20-588

Figures

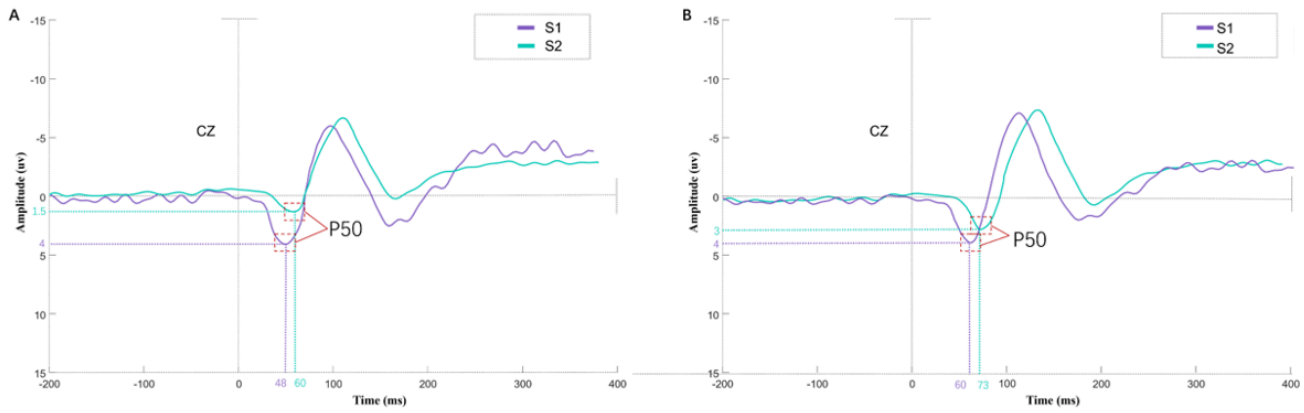


Figure 1

Comparison of P50 images between the patient group and the control group.

Note: S1 and S2 evoked P50 ERP waveforms in healthy controls and migraine patients. **(A)** shows the healthy control group, while **(B)** depicts the migraine patient group. Using the Cz electrode as an example, this figure displays the P50 component ERP waveforms elicited by paired stimuli (S1, S2) under

the paired-click paradigm. The purple waveform represents S1-evoked activity, and the cyan waveform indicates S2-evoked activity. The corresponding dashed lines mark the peak latency and amplitude positions of the P50 component. The superimposed S1 and S2 waveforms visually demonstrate the inhibitory effect of repeated stimulation: In the control group, S2 amplitude is significantly reduced compared to S1, indicating normal sensory gating function. In the migraine group, the inhibitory effect on S2 amplitude is weakened, reflecting impaired sensory gating function.

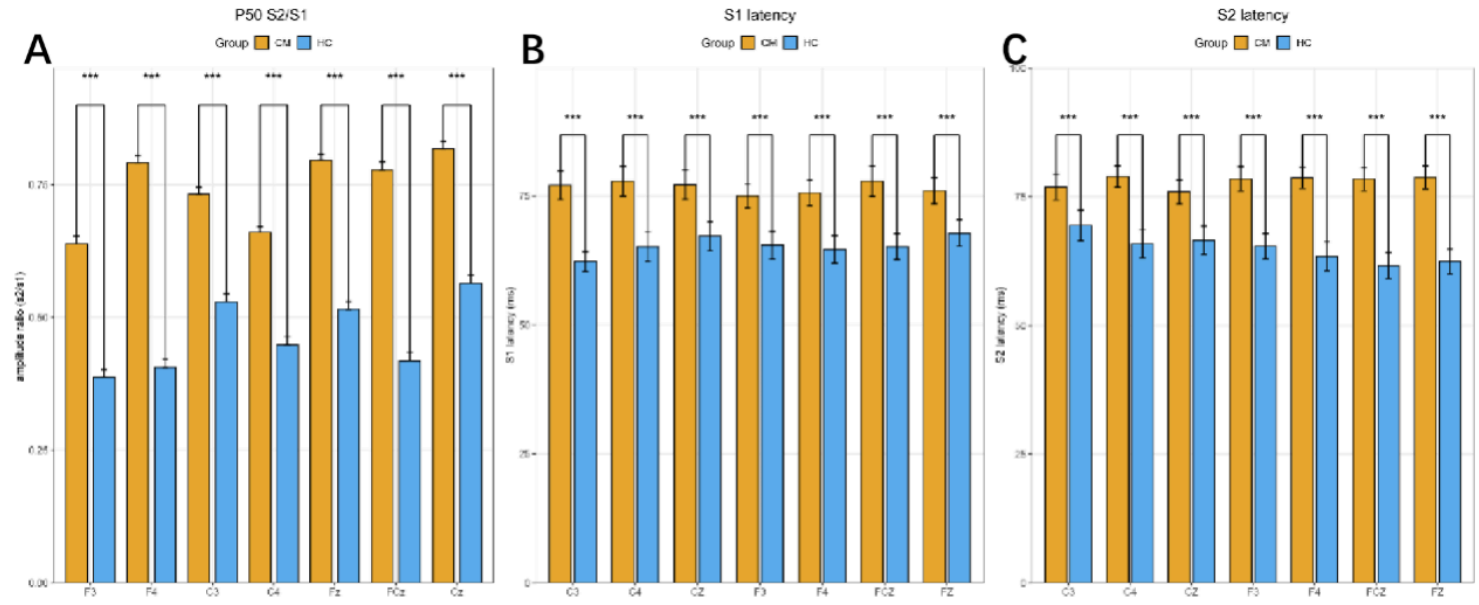


Figure 2

Comparison of incubation period and inhibition rate between CM and HC

Note: **(A)** S2/S1 ratio located in F3, F4, C3, C4, FZ, FCZ, and CZ; **(B)** S1-latency located in F3, F4, C3, C4, FZ, FCZ, and CZ; (C) S2-latency located in F3, F4, C3, C4, FZ, FCZ, and CZ (*$p < 0.05$; **$p < 0.01$; ***$p < 0.001$).

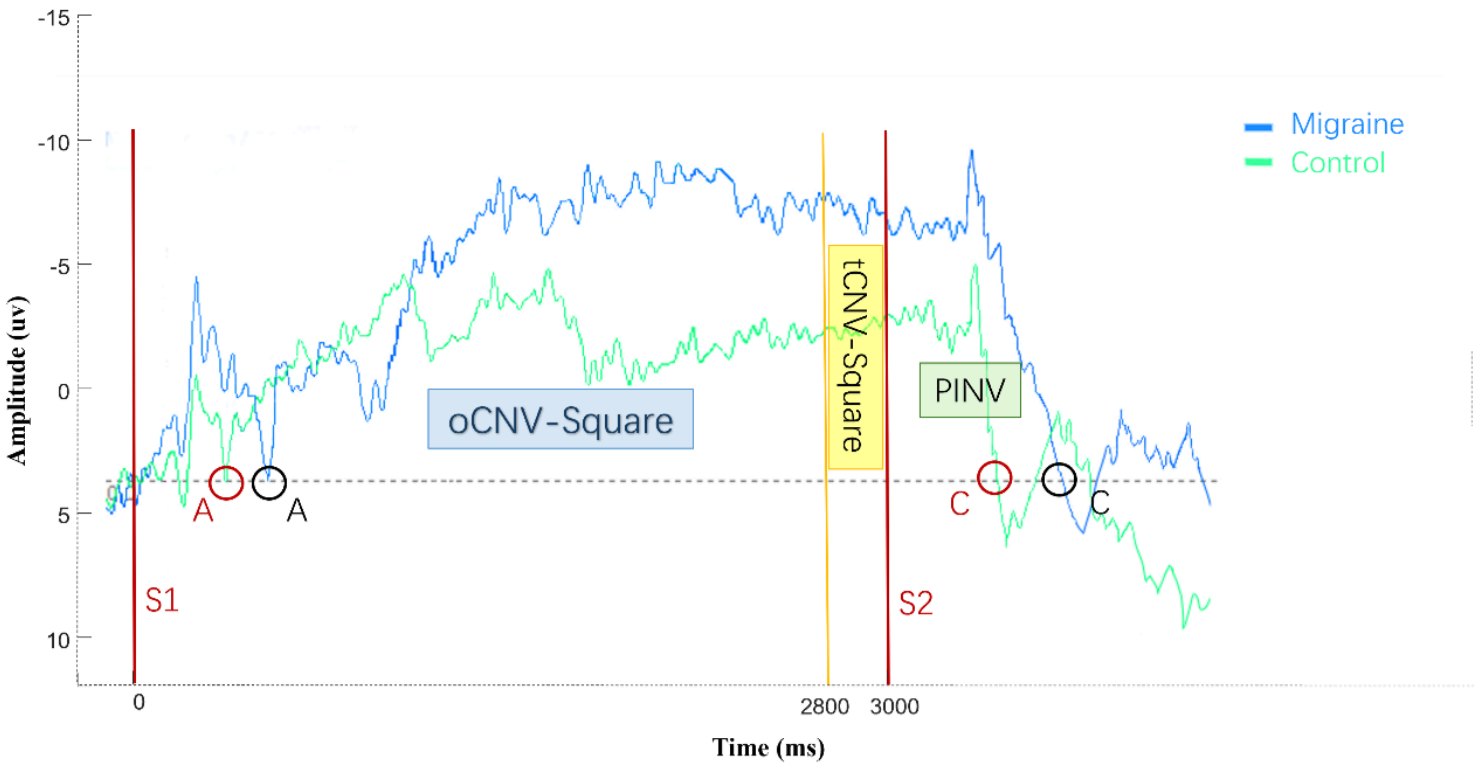


Figure 3

Examples of CNV images of CM and HC groups

Note: Under repeated auditory stimulation, compare the differences between the migraine group and the control group in terms of CNV latency, CNV amplitude, and area under the CNV curve (CNV square). Specifically, oCNV-Square is defined as the area under the curve from 0 milliseconds to 3000 milliseconds; tCNV-Square is defined as the area under the curve from 200 milliseconds (2800 milliseconds) before S2 to 3000 milliseconds; and PINV is defined as the area under the curve from after S2 (3000 milliseconds) to point C.

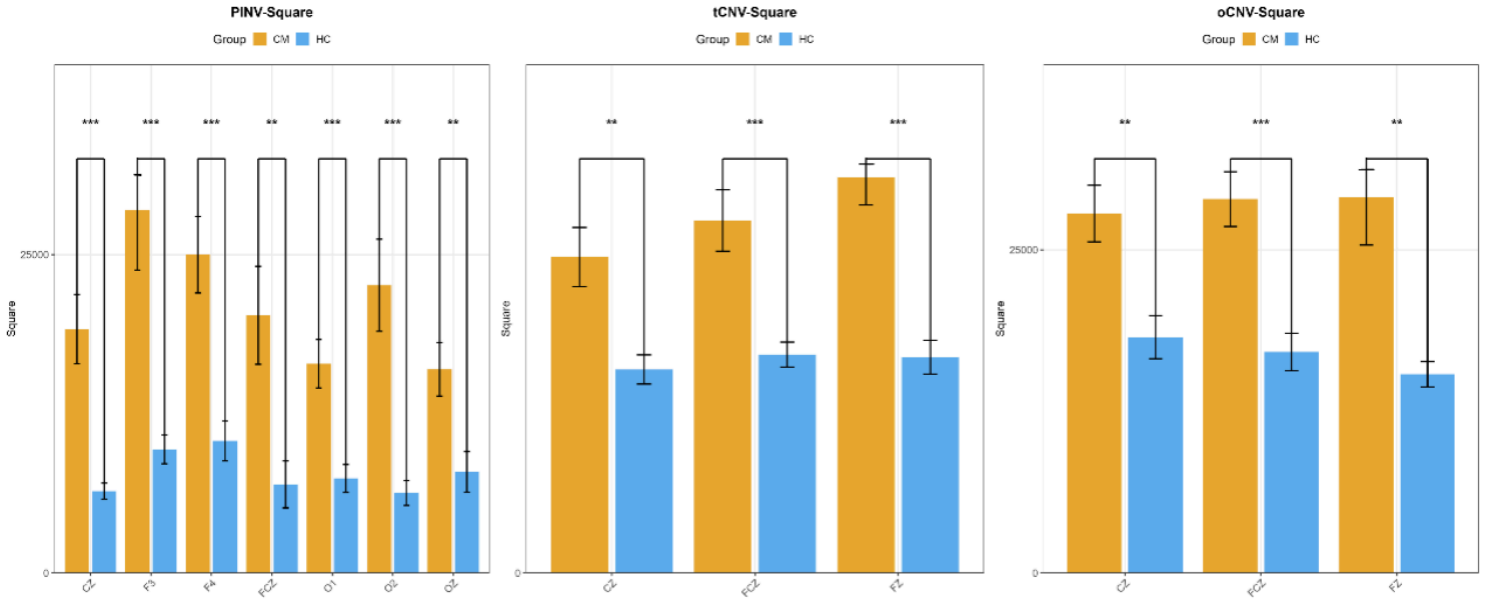


Figure 4

CM and HC area comparison chart.

Note: **(A)** PINV-Square located in CZ, F3, F4, FCZ, O1, O2, and OZ; **(B)** tCNV-Square located in CZ, FCZ, and FZ; (C) oCNV-Square located in CZ, FCZ, and FZ (*$p < 0.05$; **$p < 0.01$; ***$p < 0.001$).

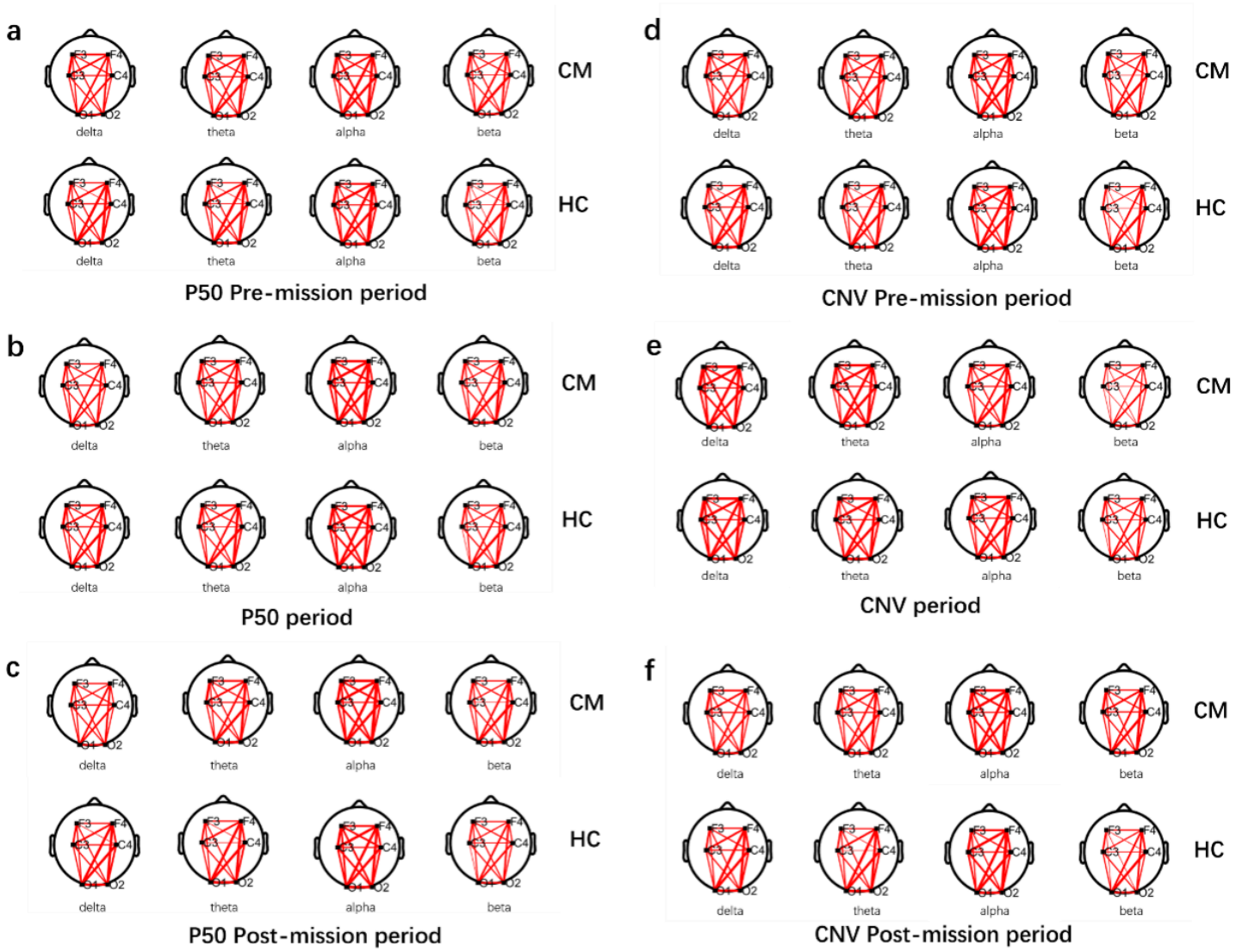


Figure 5

Functional connectivity topology distribution of CM and HC groups in six time periods.

Note: Functional connectivity topology of CM and HC groups across six conditions. (**a**) P50 Pre-task, (**b**) during the P50 task, (**c**) P50 Post-task, (**d**) CNV Pre-task, (**e**) during the CNV task, and (**f**) CNV Post-task. Line thickness indicates the strength of functional connectivity.

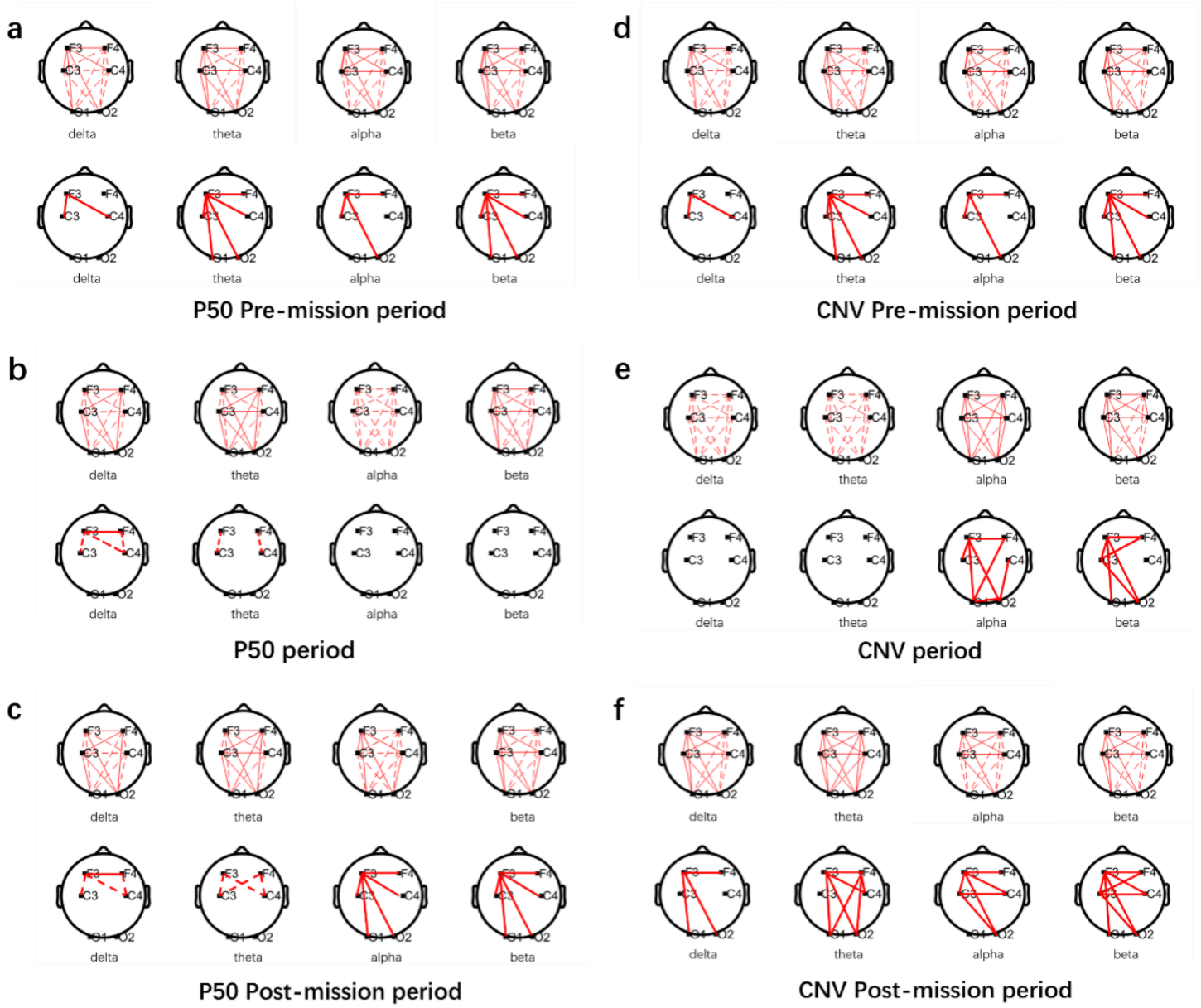


Figure 6

Differential brain network connectivity maps between the CM and HC groups at six time periods.

Note: Functional connectivity topology of CM and HC groups across six conditions. (**a**) P50 Pre-task, (**b**) during the P50 task, (**c**) P50 Post-task, (**d**) CNV Pre-task, (**e**) during the CNV task, and (**f**) CNV Post-task. Taking panel a as an example, the first row displays the group difference network between the CM and HC groups. Thicker lines denote larger between-group differences; solid lines indicate enhanced functional connectivity in the CM group relative to the HC group, whereas dashed lines indicate reduced functional connectivity in the CM group. The second row presents the topological distribution of functional connections with significant between-group differences.

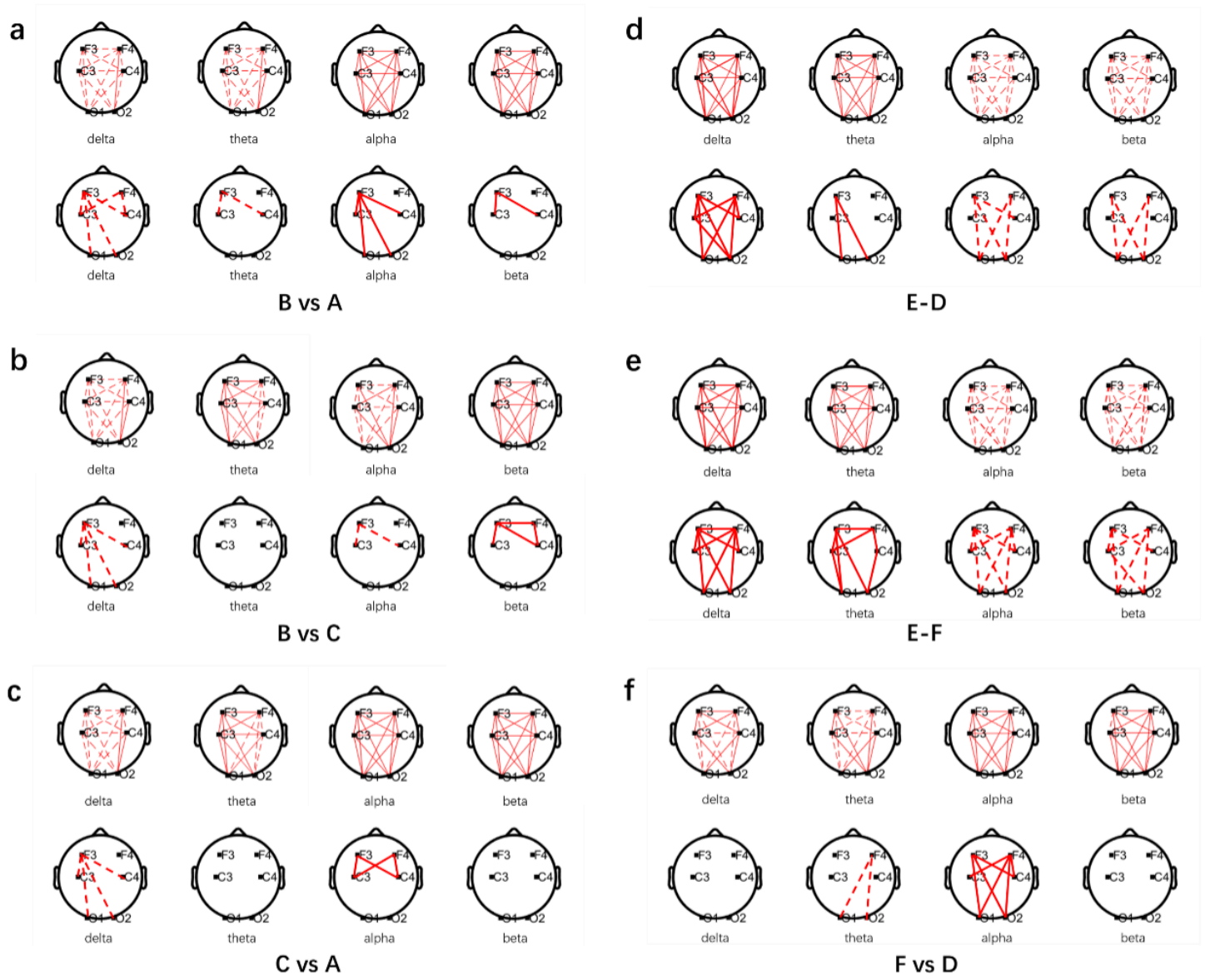


Figure 7

Functional connection topology of the CM group in different periods.

Note: Functional connectivity topologies of the CM group across different periods. (**a**) Period B vs. Period A, (**b**) Period B vs. Period C, (**c**) Period C vs. Period A, (**d**) Period E vs. Period D, (**e**) Period E vs. Period F, and (**f**) Period F vs. Period D. Taking Figure (a) as an example, the first row displays the intergroup difference network between Period B and Period A. Thicker lines indicate greater intergroup differences; solid lines indicate enhanced functional connectivity in Period B relative to Period A, while dashed lines indicate weakened functional connectivity in Period B. The second row presents the distribution of functional connectivity topologies with significant intergroup differences.

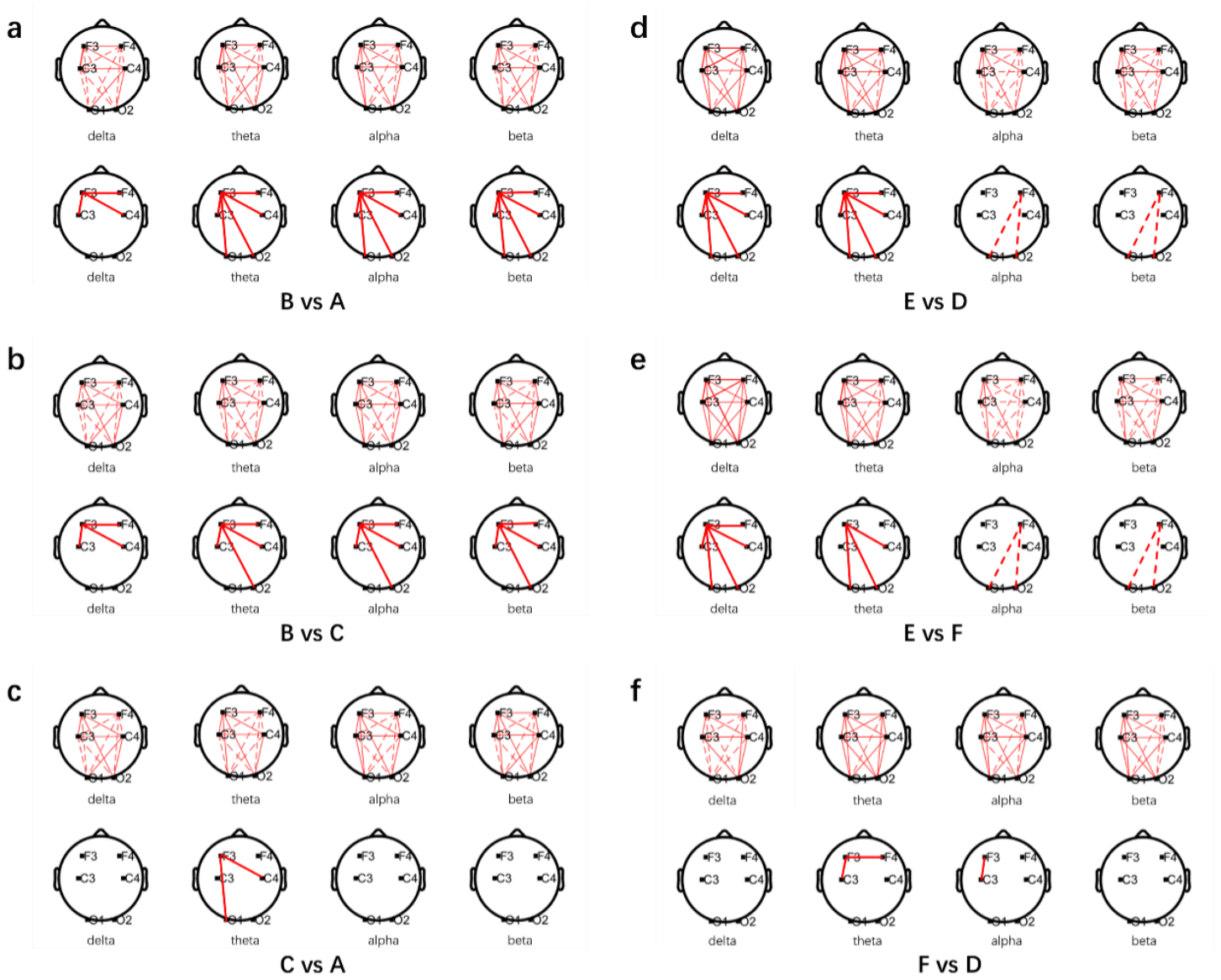


Figure 8

Functional connection topology of the CM group in different periods.

Note: Functional connectivity topologies of the HC group across different periods. (**a**) Period B vs. Period A, (**b**) Period B vs. Period C, (**c**) Period C vs. Period A, (**d**) Period E vs. Period D, (**e**) Period E vs. Period F, and (**f**) Period F vs. Period D. Taking Figure (a) as an example, the first row displays the intergroup difference network between Period B and Period A. Thicker lines indicate greater intergroup differences; solid lines indicate enhanced functional connectivity in Period B relative to Period A, while dashed lines indicate weakened functional connectivity in Period B. The second row presents the distribution of functional connectivity topologies with significant intergroup differences.